Multiple-image treatment of induced charges in Monte Carlo simulations of electrolytes near a spherical dielectric interface

Zecheng Gan and Zhenli Xu[*]

Department of Mathematics and Institute of Natural Sciences, Shanghai Jiao Tong University, Shanghai 200240, China

The polarization-induced charges of a dielectric sphere are studied for charged colloidal systems in electrolyte solutions with a primitive model. The method of constructing multiple-image charges is used to approximate the polarization potential of a microion outside the sphere; it is based on a numerical discretization of the potential's analytical integral representation, and can systematically approximate the exact potential with desired accuracy by varyiation of the number of point images. Different aspects of the image effects are then investigated by Monte Carlo simulations for several colloidal systems, in both salt-free and salty environments. Furthermore, we studied the influence of discrete surface charges of different valences, and demonstrate that the polarization charges can significantly strengthen charge reversal for the colloid-microion complex, especially for multivalent interfacial ions.

I. INTRODUCTION

Electrostatic interactions play an extremely important role in the study of the structure and functional properties of charged polymers in solution. In colloidal and biological science, the attractive or repulsive force between colloidal particles is usually controlled by the charge strength of the colloids and screened by small ions such as sodium and chloride ions present in the system. The interior of colloid particles such as latex particles, surfactant micelles, and global proteins has a low dielectric constant (typically between 2 and 5), much smaller than that of the surrounding electrolyte (about 80 for water). As the size of colloids, ranging from 10 to 10 000 Å, is larger than atomic scales, an understanding of the image effect [1–4] due to the dielectric jump is crucial to correctly predict the physicochemical properties of a colloidal system which is of both experimental and theoretical interest.

Mean-field approximations based on the Poisson-Boltzmann (PB) theory and its variants (see [5–8], to mention a few references), pioneered by Gouy and Chapman, are widely used due to the simplicity and clear physical meaning of these approximations. They are successful in describing the electrostatic interaction as long as the electrostatic coupling strength is weak, especially for electrolyte solutions containing only monovalent ions. These approximations, however, break down in interpreting the origin of charge inversion [9,10] and the attraction between like-charge objects driven by electrostatic correlations, which have been reported in a large number of experimental studies. The promising alternative is the primitive model originating from McMillan-Mayler solution theory [11], which represents the small ions in the electrolyte as mixtures of charged hard spheres with different sizes, whereas the solvent is treated by a mean-field approximation and characterized by its dielectric constant. The charged colloids and ions interact through unscreened Coulomb potentials. Analytical tools such as integral equations and density functional approaches, as well as computer simulations using molecular dynamics and Monte Carlo (MC)

methods, have been developed [12–19]. It is widely found that the primitive model can predict electrostatic correlations of the macroion (colloidal particle) with other small ions in solution, and can thus be used to study the charge inversion and like-charge attraction. Computer simulations with the primitive model are of importance for electric interactions of colloidal solutions due to the limitations of theoretical studies in treating dielectric boundaries.

Using computer simulations with the primitive model, a lot of attention has been paid to planar dielectric substrates (a single plate or two parallel plates) in contact with an electrolyte solution; the colloidal particles are considered to be large in comparison with the size of the small ions. With this approximation, the image effect due to the dielectric difference is simply taken into account by putting a point charge at the mirror location of each ion [2]. In spite of its importance, the shortcoming of the planar approximation is that the ions are not affected by the curvature of the colloidal particle, and so the approximation fails to work if the influence of the curvature is considerable. For this purpose, other geometries such as spheres or cylinders should be used.

Concerning the image effect of spherical geometries, the exact representation is the Kirkwood multipole series expansion [20], which has been applied to MC simulations [21] of colloidal systems; however, it is known that the series has a slow convergence for ions near the spherical surface and many multipoles have to be included, leading to an unacceptably high computational cost for systematic studies. Image methods have been widely employed in many biological systems, e.g., by Friedman [22], Linse [23], and Abagyan and Totrov [24]. These approximations could pose an accuracy problem for colloidal interactions because use of only one or two images to represent the polarization potential is crude and the accuracy cannot be systematically improved. The situation has motivated the development of a higher-order approximation with multiple images [25] by discretization of the exact integral representation, which can approach any desired accuracy by increase in the number of images. By extension, the idea of multiple images can also be used for the interior field calculation of the PB equations [26,27] and for

---

*xuzl@sjtu.edu.cn

cylindrical geometries [28]; see the recent review [29] for this topic.

The main objective of this paper is to investigate the polarization effect of a colloidal sphere immersed into an electrolyte solution, in which a precise and efficient treatment of polarization-induced charges is crucial. The multiple-image approximation is coupled with MC simulations to form a particle system of Coulomb interactions, which is a mixture of the ions and their images, to perform the calculation. When applied to large colloidal systems, such pairwise Coulomb interaction is useful, as many accelerating algorithms like fast Fourier transform [30] and fast multipole methods [31–34] can be used. Furthermore, by taking into account the effect of image charges, we study the charge inversion phenomenon near the colloidal surface, and illustrate that the charge inversion can be enhanced by both the multivalent discrete interfacial charges and the image charges.

The organization of the remainder of the paper is as follows. In Sec. II, we describe the computational model and the details of the MC simulations. In Sec. III, the simulation results and discussion are presented. The conclusions are drawn in Sec. IV.

II. METHOD

In our model system, a charged colloidal sphere, referred to as a macroion, is surrounded by a dielectric environment embedded with small hard spheres representing the ionic species. We first focus on the electrostatic potential around a dielectric sphere of radius a induced by a point charge outside the sphere (see Fig. 1) using the spherical coordinates $\mathbf{r} = (r, \theta, \phi)$; for convenience the charge of the spherical macroion is assumed to be zero, as if not the superposition principle can be used to add its influence. The multipole expansion and its image approximation are studied. We then discuss their application in MC simulations of a negatively charged macroion in contact with electrolytes.

A. Image representation of the polarization potential

We suppose the origin is at the center of the dielectric sphere describing the macroion. The interior of the macroion is characterized by a dielectric constant ε_{i} different from that of the surrounding solvent medium, ε_{o}. These form the
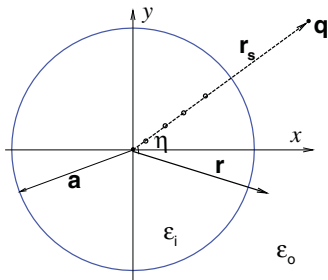

FIG. 1. (Color online) Two-dimensional schematic illustration of a dielectric sphere with a point charge outside. The polarization effect of the charge due to the dielectric discontinuity is represented by four images (empty circles); the closest one to the boundary is the Kelvin image.

dielectric function $\varepsilon(\mathbf{r})$ on the full space. Typically, $\varepsilon_{\mathrm{i}} = 2$ for a hydrocarbon substrate and $\varepsilon_{\mathrm{o}} = 78.3$ for water solvent at room temperature. The electrostatic influence of the ionic species in the solvent is treated as if they are point charges. From classical electrodynamics [35], the electric potential is described by the Poisson equation

$$-\nabla \cdot \varepsilon(\mathbf{r})\nabla \Phi(\mathbf{r}) = 4\pi\rho(\mathbf{r}), \tag{1}$$

where $\rho(\mathbf{r})$ is the charge density of free ions surrounding the macroion. Here $\rho(\mathbf{r}) = q\delta(\mathbf{r} - \mathbf{r}_s)$ for one source charge q at $\mathbf{r}_s$ outside the sphere leads to the Green's function of the inhomogeneous system by the Kirkwood multipole expansion [20].

The absence of the source charge inside the sphere reduces Eq. (1) to the Laplace equation, $\Delta \Phi = 0$, for $r < a$. By azimuthal symmetry, the Laplace equation can be written as

$$\frac{1}{r^2}\frac{\partial}{\partial r}\left(r^2\frac{\partial \Phi}{\partial r}\right) + \frac{1}{r^2 \sin \eta}\frac{\partial}{\partial \eta}\left(\sin \eta \frac{\partial \Phi}{\partial \eta}\right) = 0, \tag{2}$$

where η is the angle between $\mathbf{r}$ and $\mathbf{r}_s$ and satisfies $\cos \eta = \cos \theta \cos \theta_s + \sin \theta \sin \theta_s \cos(\phi - \phi_s)$. The general solution for the potential inside the sphere can then be described in terms of spherical harmonics,

$$\Phi(\mathbf{r}) = \sum_{n=0}^{\infty} A_n r^n P_n(\cos \eta), \tag{3}$$

where $P_n(\cdot)$ is the Legendre polynomial of order n.

Outside the dielectric sphere, the solution can be described by

$$\Phi(\mathbf{r}) = \Phi_{\mathrm{Coul}}(\mathbf{r}) + \Phi_{\mathrm{pol}}(\mathbf{r}), \tag{4}$$

where $\Phi_{\mathrm{Coul}} = q/\varepsilon_{\mathrm{o}}|\mathbf{r} - \mathbf{r}_s|$ is the direct Coulomb potential in the homogeneous solvent, and Φ_{pol} is the polarization potential, also known as the image correction, due to the dielectric jump on the spherical surface. Applying the multipole expansion of the reciprocal distance, the general form of the potential $\Phi(\mathbf{r})$ reads

$$\Phi(\mathbf{r}) = \frac{q}{\varepsilon_{\mathrm{o}}}\sum_{n=0}^{\infty}\frac{r_<^n}{r_>^{n+1}}P_n(\cos \eta) + \frac{q}{\varepsilon_{\mathrm{o}}}\sum_{n=0}^{\infty}\frac{B_n}{r^{n+1}}P_n(\cos \eta), \tag{5}$$

where we have used the harmonic property of Φ_{pol}, and $r_< (r_>)$ is the smaller (larger) of r and r_s.

Now we choose the constant coefficients A_n and B_n so that the potentials inside and outside the sphere satisfy the boundary conditions on the interface. The boundary conditions are the continuities of the potential and the dielectric displacement,

$$\Phi_{\mathrm{in}} = \Phi_{\mathrm{out}} \quad \text{and} \quad \varepsilon_{\mathrm{i}}\frac{\partial \Phi_{\mathrm{in}}}{\partial r} = \varepsilon_{\mathrm{o}}\frac{\partial \Phi_{\mathrm{out}}}{\partial r}, \tag{6}$$

which lead to a set of two linear equations for each n,

$$a^n A_n = \frac{a^n}{r_s^{n+1}} + \frac{1}{a^{n+1}}B_n,$$
$$\frac{\varepsilon_{\mathrm{i}}}{\varepsilon_{\mathrm{o}}}na^{n-1}A_n = \frac{na^{n-1}}{r_s^{n+1}} - \frac{n+1}{a^{n+2}}B_n, \tag{7}$$

TABLE I. Truncation terms for the multipole expansion and numbers of point images (discrete images for the integral plus the Kelvin image) required to obtain relative errors less than 0.1% and 0.01% in the self-energy calculation of a charge at r_s. The dielectric constants inside and outside the sphere are 2 and 78.3, respectively.

r_s/a	0.1% error		0.01% error	
	Multipoles	Images	Multipoles	Images
1.02	178	8	236	11
1.04	91	7	121	9
1.06	62	6	82	8
1.08	48	6	63	7
1.1	39	5	51	7
1.2	21	4	28	5
1.3	15	4	20	5
1.4	12	4	16	5
1.5	11	4	13	4
1.6	9	4	12	4

and its solution is given by

$$A_n = \frac{1}{r_s^{n+1}} \frac{(2n+1)\varepsilon_o}{n\varepsilon_i + (n+1)\varepsilon_o},$$
$$B_n = \frac{a^{2n+1}}{r_s^{n+1}} \frac{n(\varepsilon_o - \varepsilon_i)}{n\varepsilon_i + (n+1)\varepsilon_o}. \tag{8}$$

The polarization potential is then obtained:

$$\Phi_{\mathrm{pol}}(\mathbf{r}) = \frac{q}{\varepsilon_o} \sum_{n=0}^{\infty} \frac{a^{2n+1}}{(rr_s)^{n+1}} \frac{n(\varepsilon_o - \varepsilon_i)}{n\varepsilon_i + (n+1)\varepsilon_o} P_n(\cos\eta). \tag{9}$$

A straightforward way to compute this expression is to truncate the infinite series into a finite sum. Usually, the series converges quickly for the source charge is far from the boundary. The convergence is slow, however, for charges near the spherical surface, as shown in Table I, requiring a large number of truncation terms in Eq. (9), and, as a result, limiting practical calculations. The method based on the line image representation is more efficient and gives an alternative and simpler analytical way.

By a simple derivation based on the harmonic expansion of the reciprocal distance, Eq. (9) can be reformulated [25,36–39] as the sum of contributions from a Kelvin image, q_{K}, and a line image from the origin to the Kelvin image point, $\mathbf{r}_{\mathrm{K}} = \mathbf{r}_s a^2/r_s^2$,

$$\Phi_{\mathrm{pol}}(\mathbf{r}) = \frac{q_{\mathrm{K}}}{\varepsilon_o|\mathbf{r} - \mathbf{r}_{\mathrm{K}}|} + \int_0^{r_{\mathrm{K}}} \frac{q_{\mathrm{line}}(x)}{\varepsilon_o|\mathbf{r} - \mathbf{x}|} dx, \tag{10}$$

where $\mathbf{x} = x\mathbf{r}_s/r_s$, and the strengths of the Kelvin image and the line image are given by

$$q_{\mathrm{K}} = -\frac{\gamma a}{r_s} q \quad \text{and} \quad q_{\mathrm{line}}(x) = \frac{\gamma \sigma q}{a} \left(\frac{r_{\mathrm{K}}}{x}\right)^{1-\sigma},$$

with the parameters $\gamma = \frac{\varepsilon_i - \varepsilon_o}{\varepsilon_i + \varepsilon_o}$ and $\sigma = \frac{\varepsilon_o}{\varepsilon_i + \varepsilon_o}$. The idea of the line image representation was originally given in the 19th century by Neumann [40] and redeveloped several times by several authors in various fields of application, as summarized by Lindell [41].

To obtain a highly accurate approximation with discrete point images, we use the idea of the multiple-image approxi-

mation [25]. The I-point Gauss-Legendre quadrature is used to approximate the line integral, leading us to

$$\Phi_{\mathrm{pol}}(\mathbf{r}) = \frac{q_{\mathrm{K}}}{\varepsilon_o|\mathbf{r} - \mathbf{r}_{\mathrm{K}}|} + \sum_{m=1}^{I} \frac{q_m}{\varepsilon_o|\mathbf{r} - \mathbf{x}_m|}, \tag{11}$$

with the charge strengths $q_m = \frac{\omega_m}{2}\frac{\gamma a q}{r_s}$ and locations $x_m = r_{\mathrm{K}}(\frac{1-s_m}{2})^{1/\sigma}$, where $\{\omega_m, s_m, m = 1, 2, \ldots, I\}$ are the I-point Gauss weights and locations on the interval $[-1, 1]$. If we let $q_0 = q_{\mathrm{K}}$ and $\mathbf{x}_0 = \mathbf{r}_{\mathrm{K}}$, the approximate potential reads

$$\Phi_{\mathrm{pol}}(\mathbf{r}) = \sum_{m=0}^{I} \frac{q_m}{\varepsilon_o|\mathbf{r} - \mathbf{x}_m|}, \tag{12}$$

which is a total of $I + 1$ point images. A schematic illustration of the image charges is plotted in Fig. 1, where the images are symbolized with empty circles.

The number of images, $I + 1$, is determined by the desired accuracy. In Table I, comparable results are given for the self-polarization-energy of a point charge outside the sphere, $q\Phi_{\mathrm{pol}}(\mathbf{r}_s)/2$, as a function of the ratio r_s/a, calculated by two methods. One is by direct truncation of the series of the multipole expansion (9). The other is the method of images. It is shown that only a few image charges can provide a very accurate approximation; thus the method will be very useful for simulations of large particle systems.

B. Monte Carlo simulations

We have employed canonical-ensemble Metropolis MC simulations [42,43] based on the primitive model for a solution in the presence of a negatively charged dielectric colloidal sphere and microions. The method of multiple images for the charged hard-sphere system of the macroion and N small microions is used to describe the image effect of the counterions and coions due to the dielectric boundary. The spherical macroion is of radius a, and a bare charge $Q = -Z_M e$ is placed at the center (origin) or discretely distributed on the surface. The microions are used to ensure the electroneutrality of the system and represent the salt concentration; all of them are of diameter τ and have charge $q_i = \pm Z e$ for $i = 1, \ldots, N$, Z being the valence of the ion. We use $(I - 1)$-point quadrature for the line image, so each microion is accompanied by I image charges. Overall, there are $N \times I$ images.

For a uniformly charged colloidal surface, the total potential energy of the system, i.e., the Hamiltonian, is expressed as a sum of three contributions,

$$U = \sum_{i=1}^{N} \left(U_i^{\mathrm{ms}} + \sum_{j=i+1}^{N} U_{ij}^{\mathrm{ss}} + \sum_{j=1}^{N} \sum_{\mathrm{im}=0}^{I-1} U_{ij}^{\mathrm{im}} \right). \tag{13}$$

The first term represents the interaction between the macroion and the source ions,

$$U_i^{\mathrm{ms}} = \begin{cases} \frac{l_B}{\beta e^2} \frac{Q q_i}{r_i} & \text{for} \quad r_i \geqslant a + \frac{\tau}{2}, \\ \infty & \text{for} \quad r_i < a + \frac{\tau}{2}, \end{cases} \tag{14}$$

where $l_B = \beta e^2/(4\pi\varepsilon_0\varepsilon_o)$ is the Bjerrum length and ε_0 is the vacuum permittivity. $\beta = 1/k_B T$ is the inverse thermal energy

with k_B being the Boltzmann constant and T the temperature. At room temperature, $l_B = 7.14$ Å for water. The second term in Eq. (13) represents the interaction between source charges, which is the Coulomb potential plus a hard-sphere potential,

$$U_{ij}^{ss} = \begin{cases} \frac{l_B}{\beta e^2} \frac{q_i q_j}{r_{ij}} & \text{for} \quad r_{ij} \geqslant \tau, \\ \infty & \text{for} \quad r_{ij} < \tau. \end{cases} \quad (15)$$

The last term in Eq. (13) describes the contribution from the interaction between the images and source ions, given by

$$U_{ij}^{im} = \begin{cases} \left(1 - \frac{\delta_{ij}}{2}\right) \frac{l_B}{\beta e^2} \frac{q_i q_j^{im}}{|\mathbf{r}_i - \mathbf{r}_j^{im}|} & \text{for} \quad r_i \geqslant a + \frac{\tau}{2}, \\ \infty & \text{for} \quad r_i < a + \frac{\tau}{2}, \end{cases} \quad (16)$$

where δ_{ij} is the Kronecker delta, and q_j^{im} and $\mathbf{r}_j^{im}$ are the charge strength and location of the im-th one of I images of charge j.

III. RESULTS AND DISCUSSION

In the simulations, the following parameters are assumed throughout the paper: $\varepsilon_i = 2$, $\varepsilon_o = 78.3$, and $T = 300$ K. The microion diameter is $\tau = 3.57$ Å, and the colloidal radius is set to be $a = 30$ Å. The spherical cell model [44] is used to define the boundary of the electrolyte solution, which introduces an infinite external potential to the system if a small ion moves outside the cell. The radius of the spherical cell is denoted by R_{cell}, which takes the value $R_{cell} = 20\tau$ so that the volume fraction of the macroion remains a constant.

Seven colloidal systems are used to test the simulation aspects with the image effect. Systems I and II have the same valence of the macroion, $Z_M = 80$. System I has monovalent counterions, $Z = 1$, and system II divalent counterions, $Z = 2$. The valence of systems III–VII is also fixed with $Z_M = 160$ and with divalent counterions and coions and varying salt concentration.

The MC results are depicted using the macroion-microion radial distribution function (RDF) and the integrated charge distribution function (ICDF) by calculating the bulk densities of the counterions and coions. The RDF of each ionic type is given by

$$g_{\pm}(r) = \frac{\langle N_{\pm}(r, r + \Delta r) \rangle}{\frac{4}{3}\pi[(r + \Delta r)^3 - r^3]}, \quad (17)$$

normalized by $\int_a^{R_{cell}} \pi r^2 g(r) dr$, where $N_{\pm}(r, r + \Delta r)$ is the particle number in the spherical shell between r and $r + \Delta r$, and $g(r) = g_+(r) + g_-(r)$ is the sum of the RDFs of counterions and coions. The angular bracket $\langle \cdot \rangle$ represents an average over all the bins. The ICDF describes the total charge distribution along the radial direction, which is defined by

$$Q(r) = Q_M + Z[N_+(a,r) - N_-(a,r)]. \quad (18)$$

Generally, $Q(r)$ increases from Q_M to 0 when r changes from a to the cell radius R_{cell}. Charge inversion happens if $Q(r)$ reverses its sign somewhere.

A. Dependence of accuracy on the number of images

We first investigate the influence of varying image number for systems I and II, the cases with zero salt concentration. In the calculations, the image number I increases from 0 to 8. By $I = 0$, we mean that there is no image present, $\Phi_{pol} = 0$, which represents the case when the dielectrics inside and outside the sphere are the same. When $I = 1$, only the Kelvin image is considered, and when $I = 2$, the effect of the line image is taken into account.

The profiles of the RDFs and ICDFs near the colloidal spheres of these two systems are plotted in Fig. 2. Presumably, at least two images have to used in order to take into account the polarization effect as well as to retain the electrical neutrality of the image charges. It is found that it is important to take into account the image effect in order to correctly determine the counterion distribution, in particular for multivalent counterions. We see that the results break down if only the Kelvin image is present, demonstrating that treatment of the line image is necessary. It is also shown that three to four images are enough to provide a convergent approximation to the image effect, in agreement with the self-energy calculation for one ion shown in Table I. The RDF curves overlap for $I = 3$ to 8 even in the enlarged subplots, showing the fast convergence. This is very advantageous in comparison to the direct multipole expansion for which one has to use dozens or even hundreds of terms for convergence of the desired accuracy.

B. Charge inversion for uniformly charged surface

Charge inversion (also called overcharging or charge reversal) occurs when a highly charged macroion is immersed in a solution with multivalent conterions and the interfacial charge is overcompensated by the counterions, so that the effective charge of the macroion-microion complex is inverted. This charge inversion has been demonstrated in experiments on many different systems [45,46]. The traditional PB theory fails to describe it, and thus the explanation of charge inversion has motivated a lot of theoretical and computational investigation as it could be relevant in many physical and biological problems such as the like-charge attraction between DNA rods [9]. A number of theories [10], such as integral equations, field theoretic calculations, and density functional theory, have been developed to describe this phenomenon, as well as molecular dynamics and MC simulations [21,47–50] which confirm the theoretical predictions. In the simulations of this paper, we aimed to verify the performance of the method of images through simulating this phenomenon and to study the effect of the image charges of the overcharging by considering discrete interfacial charges in Sec. III C.

We simulate the charge inversion phenomenon by investigating the salt effect on the ion distribution with systems III–VII, which are composed of a macroion of $Z_M = 160$ and divalent salt ions. The divalent counterion numbers of the five systems are $N_c = 80, 180, 280, 380$, and 480, respectively. 80 counterions correspond to a concentration of 87 mM, and thus the five systems have concentrations from 87 to 522 mM for conterions and 0 to 435 mM for coions.

In the calculations, three images are used to represent the image effect of each ion. The results for the RDFs and ICDFs are illustrated in Fig. 3, where those without
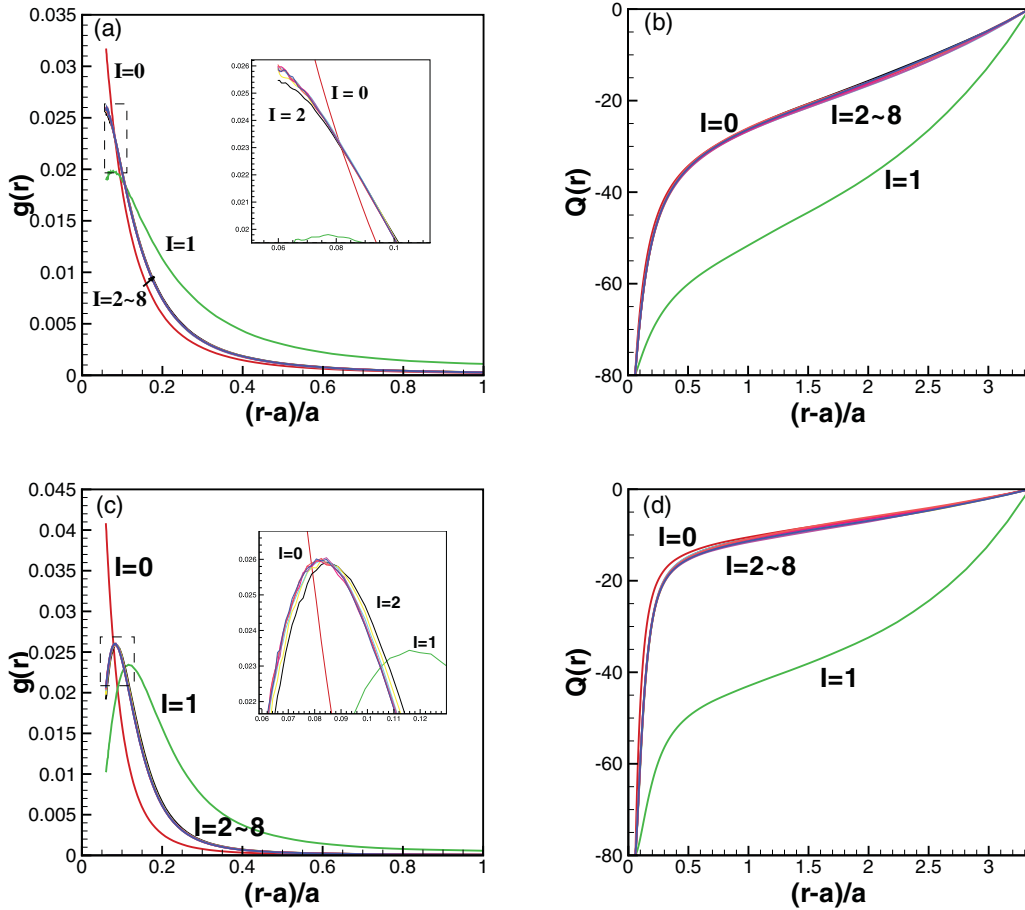
FIG. 2. (Color online) Radial distribution and integrated charge distribution functions of systems I (a), (b) and II (c), (d) with increasing number of images from $I = 0$ to 8. The insets in (a) and (c) are enlargements of the corresponding dashed region.

the image effect taken into account are also included for comparison. It can be seen that the inverted charge Q_{inv} (the maximum of each ICDF curve) increases montonically with growing salt concentration. The overcharging starts at $N_c = 280$ with the inverted charge $Q_{inv} = 1.32\,e$ and goes to $8.57\,e$ when $N_c = 480$. The image effect can weaken the overcharging effect, mostly because of the repulsive effect between the image charges and the microions. These results are in agreement with a thorough study of the polarization effect of spherical macroions performed by Messina [21]; thus the accuracy of the image method is shown to be reasonable although only three images are used for each ion.

All calculations are performed on a Linux machine with 2.67 GHz CPU and 48 Gbytes of memory. In each simulation, the program runs 1×10^6 trial moves per particle, without parallel acceleration. Accounting for the image effect, the CPU times from system III with 80 microions to system VII with 880 microions go from 20 to 2300 min (around 37.8 h), scaling as $O(N^2)$. As the particle system composed of microions and their images is in Coulomb form, this computational complexity can be reduced if linear-scaling fast algorithms are introduced to speed up the particle interactions, and thus this image method for treating the surface polarization can be useful to study systems of larger scale, which will be the objective of our ongoing project.

C. Image effect on discrete surface charge

For a single spherical macroion, the bare charge is represented by a central charge, which is equivalent to a uniformly charged macroion surface. However, the charges are discretely localized in nature in the form of interfacial groups whose charges range from $-1e$ to $-4e$ [51]. The distribution of surface charges could play an important role in the counterion distribution near the surface. The effect of discrete macroion charge distribution has been studied in recent years [52–54]. However, the image effect of the discrete surface charge has been less investigated. In fact, if the macroion is modeled by a uniformly distributed surface charge, then the image effect of the surface charge vanishes due to symmetry. But if the surface charge is discrete and randomly distributed on the surface, the symmetry no longer exists. We study the effect of discrete surface charges on charge inversion with different head group valences through MC simulations, taking into account the image effect.

The discrete colloidal charges are represented by small ions of diameter τ (the same as the counterion's diameter), which are randomly distributed on the surface of the macroion. The total charge of the macroion is $Q_M = q_D N_D$, where $q_D = -Z_D e$, Z_D is the valence of the discrete interfacial ions, and N_D is their number. These discrete ions are embedded in the colloidal sphere with their centers at its surface. Figure 4 is a
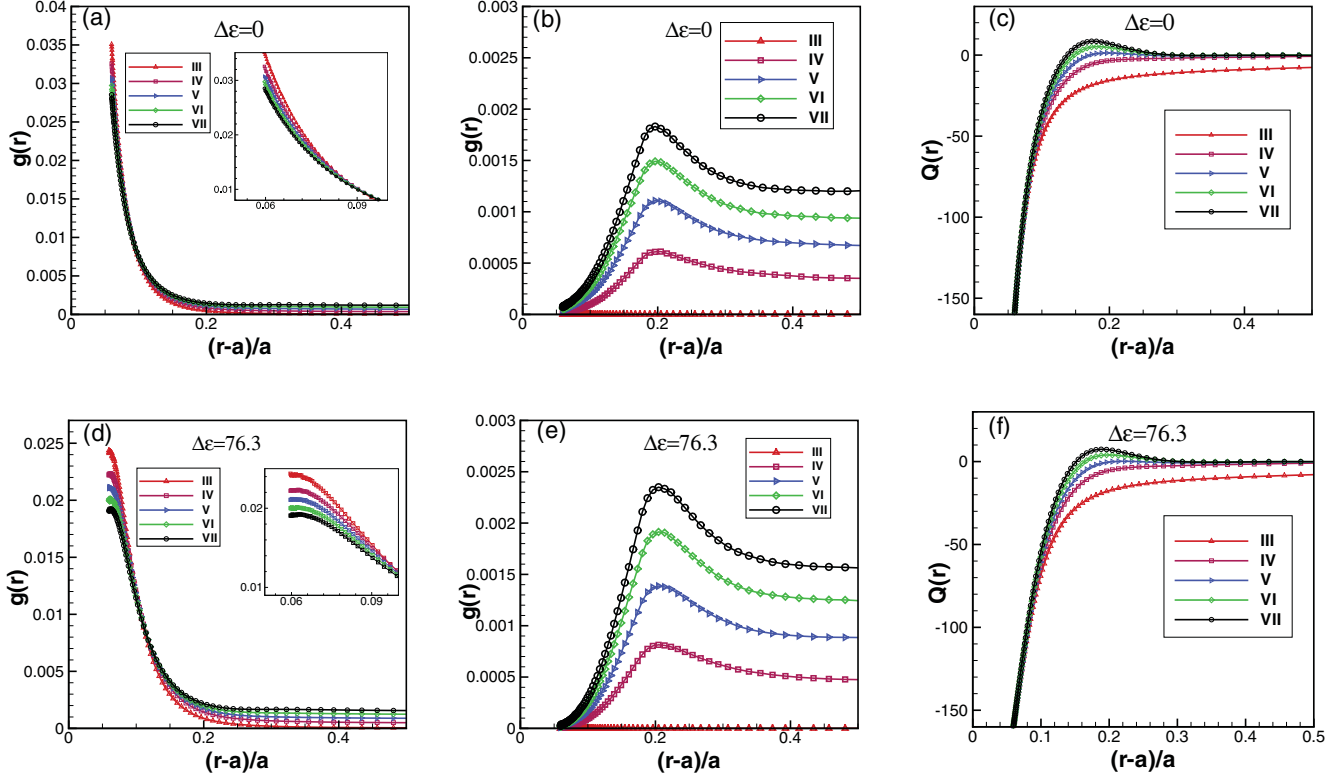
FIG. 3. (Color online) Radial distribution and integrated charge distribution functions of systems III-VII, where (a), (d) are the counterion RDFs, (b), (e) are the coion RDFs, and (c), (f) are the ICDFs. Three images are used to approximate the polarization potential of each ion.

schematic view of the setup, where each interfacial charge and its Kelvin image overlap each other. In the MC simulations, the term for the macroion-microion interaction U_i^{ms} in the Hamiltonian Eq. (13) is changed into the following form:

$$U_i^{ms} = \sum_{n=1}^{N_D} U_{ni}^{ms},\qquad(19)$$

where the interaction between the ith microion and nth interfacial ion is given by

$$U_{ni}^{ms} = \begin{cases} \infty & \text{for} \quad r_i < a + \frac{\tau}{2} \quad \text{or} \quad r_{ni}^{ms} < \tau, \\ \frac{l_B}{\beta e^2}\left(\frac{q_D q_i}{r_{ni}^{ms}} + \sum_{im=0}^{I-1}\frac{q_D^{im} q_i}{r_{n,im,i}^{ms}}\right) & \text{otherwise.} \end{cases}\qquad(20)$$

Here r_{ni}^{ms} is their distance apart, q_D^{im} is the image charge of the interfacial ion, and $r_{n,im,i}^{ms}$ is the distance between the image charge and the ith microion.

We investigate the same five systems as previously studied (systems III–VII), which are composed of a macroion of $Z_M = 160$ and divalent salt ions, i.e., the salt concentration ranges from 0 to 435 mM. The only difference is that the surface charge of the macroion is discrete, and randomly distributed, with the four different valences $Z_D = 1, 2, 3.019,$ and 4. In calculations, three images are used to represent the image effect of both the salt ions and the discrete interfacial charges. We run four different random surface distributions to obtain the average inverted charge Q_{inv} for each system with a certain Z_D. The resulting differences in the inverted charge Q_{inv} compared with the previous simulation results are illustrated in Fig. 5,

where those obtained without taking account of the image effect are also shown for comparison.

Without accounting for the image effect [Fig. 5(a)], it is shown that the discrete representation of the surface charge with monovalent ions has smaller strengths of the inverted charge than the uniform surface charge, mostly because the macroion has a larger volume with the presence of interfacial ionic balls. The results for $Z_D = 2$ almost overlap with those for the uniform surface charge, and higher valences of interfacial ions cause stronger overcharging. With the image effect, the overcharging for $Z_D = 1$ is strengthened and the inverted charges are close to those for the uniform colloidal charge. This is reasonable because the Kelvin image of the
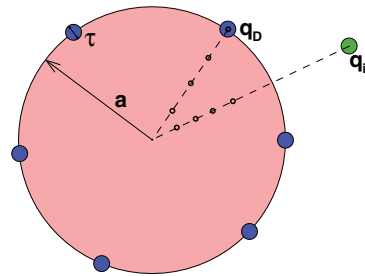

FIG. 4. (Color online) Two-dimensional schematic view of the setup: The discrete interfacial charges are in blue. The macroion of radius a is in red. The microion in the electrolyte is the full green circle. The image charges of both the microion and the interfacial ion are represented by empty circles, where the interfacial ion is overlapping with its Kelvin image.
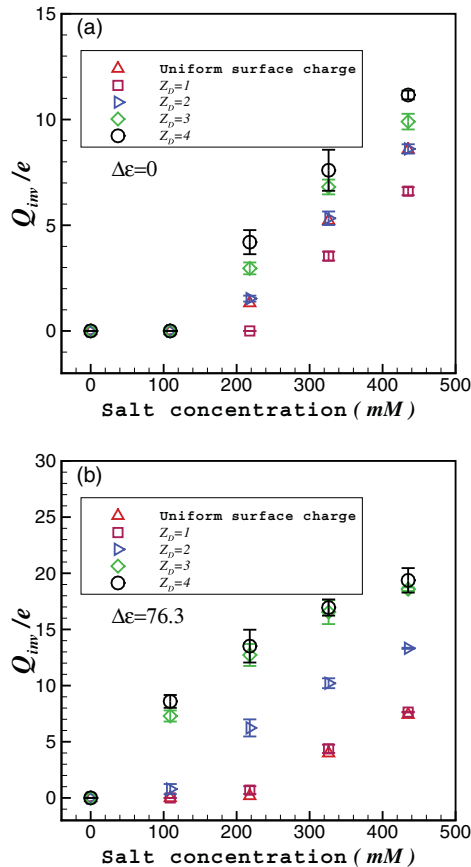
FIG. 5. (Color online) The inverted charge Q_{inv} for systems III–VII with different Z_D, where (a) does not account for the image effect, while (b) uses three image charges to represent the polarization potential of each ion. The error bar represents the maximum deviation of the four data points from their mean.

interfacial charge has the same sign as its source charge and thus has the effect of improving the attraction to counterions (see Fig. 4), even though the mobile ions and their images repel each other. From Fig. 5(b), it can be seen that Q_{inv} also gets larger for a larger Z_D, and we can conclude that the inverted charge is significantly increased when the interfacial charges have higher valence. Impressively, the presence of

dielectric images further enhances charge inversion when the surface charge is discrete; for example, when $Z_D = 4$ the Q_{inv} of system VII equals $11.16\,e$ without the image effect, and becomes $19.37\,e$ when image charges are present. This is in contrast with previous studies [14,21] reporting that the image effect weakens the degree of charge inversion, although the weakening of the overcharging is true for the uniform surface charge in the present study (see the triangle symbols in Fig. 5).

IV. CONCLUSION

In summary, we have studied the image effect for ions near a spherical macroion with MC simulations by using the method of multiple images with different numbers of images. The treatment with the image charges transforms the inhomogeneous system into a pairwise Coulomb system composed of the source and image charges, which allows for efficient calculation. The accuracy and efficiency of the algorithm are demonstrated through some colloidal systems; it is shown that only three images can provide an accurate approximation to the polarization effect of a source ion, and that the calculation of a relatively large system can be run on a desktop machine in dozens of hours.

We investigated the image effect on the charge inversion of the macroion for both a uniform surface charge and discrete charges. It is revealed that taking the image effect into account weakens the degree of the inverted charge for the uniform surface charge, but significantly strengthens it for discrete surface charges if the interfacial ions are of high valence. This is mostly because the charges of the interfacial ion and its Kelvin image overlap each other and the other images are buried inside the colloidal sphere, leading to an enhanced attraction to counterions.

[1] Y. Levin, Rep. Prog. Phys. **65**, 1577 (2002).

[2] M. M. Hatlo and L. Lue, Soft Matter **4**, 1582 (2008).

[3] R. Messina, J. Phys.: Condens. Matter **21**, 113101 (2009).

[4] R. H. French *et al.*, Rev. Mod. Phys. **82**, 1887 (2010).

[5] P. Debye and E. Hückel, Phys. Z. **24**, 185 (1923).

[6] I. Borukhov, D. Andelman, and H. Orland, Phys. Rev. Lett. **79**, 435 (1997).

[7] J. Wang, C. Tan, Y. H. Tan, Q. Lu, and R. Luo, Commun. Comput. Phys. **3**, 1010 (2008).

[8] A. R. J. Silalahi, A. H. Boschitsch, R. C. Harris, and M. O. Fenley, J. Chem. Theory Comput. **6**, 3631 (2010).

[9] A. Y. Grosberg, T. T. Nguyen, and B. I. Shklovskii, Rev. Mod. Phys. **74**, 329 (2002).

[10] H. Boroudjerdi, Y.-W. Kim, A. Naji, R. R. Netz, X. Schlagberger, and A. Serr, Phys. Rep. **416**, 129 (2005).

[11] W. G. McMillan and J. E. Mayer, J. Chem. Phys. **13**, 276 (1945).

[12] G. M. Torrie, J. P. Valleau, and G. N. Patey, J. Chem. Phys. **76**, 4615 (1982).

[13] R. Kjellander and S. Marčelja, Chem. Phys. Lett. **112**, 49 (1984).

[14] T. T. Nguyen, A. Y. Grosberg, and B. I. Shklovskii, J. Chem. Phys. **113**, 1110 (2000).

[15] D. Boda, D. Gillespie, W. Nonner, D. Henderson, and B. Eisenberg, Phys. Rev. E **69**, 046702 (2004).

[16] M. Valiskó, D. Boda, and D. Gillespie, J. Phys. Chem. C **111**, 15575 (2007).

[17] L. B. Bhuiyan, C. W. Outhwaite, and D. J. Henderson, Mol. Phys. **107**, 343 (2009).

[18] Z. Y. Wang and Y. Q. Ma, J. Chem. Phys. **131**, 244715 (2009).

[19] Z. Y. Wang and Y. Q. Ma, J. Chem. Phys. **133**, 064704 (2010).

[20] J. G. Kirkwood, J. Chem. Phys. **2**, 351 (1934).

[21] R. Messina, J. Chem. Phys. **117**, 11062 (2002).

[22] H. L. Friedman, Mol. Phys. **29**, 1533 (1975).

[23] P. Linse, J. Phys. Chem. **90**, 6821 (1986).

[24] R. Abagyan and M. Totrov, J. Mol. Biol. **235**, 983 (1994).

[25] W. Cai, S. Deng, and D. Jacobs, J. Comput. Phys. **223**, 846 (2007).

[26] Z. Xu, S. Deng, and W. Cai, J. Comput. Phys. **228**, 2092 (2009).

[27] S. Deng and W. Cai, Commun. Comput. Phys. **2**, 1007 (2007).

[28] Z. Xu, W. Cai, and X. Cheng, Commun. Comput. Phys. **9**, 1056 (2011).

[29] Z. Xu and W. Cai, SIAM Rev. (to be published).

[30] A. Arnold and C. Holm, Adv. Polym. Sci. **185**, 59 (2005).

[31] L. Greengard and V. Rokhlin, J. Comput. Phys. **73**, 325 (1987).

[32] H. Cheng, L. Greengard, and V. Rokhlin, J. Comput. Phys. **155**, 468 (1999).

[33] L. Ying, G. Biros, and D. Zorin, J. Comput. Phys. **196**, 591 (2004).

[34] B. Lu, X. Cheng, J. Huang, and J. A. McCammon, Proc. Natl. Acad. Sci. USA **103**, 19314 (2006).

[35] J. D. Jackson, *Classical Electrodynamics*, 3rd ed. (John Wiley & Sons, New York, 2001).

[36] I. V. Lindell, Radio Sci. **27**, 1 (1992).

[37] W. T. Norris, IEE Proc. Sci. Meas. Technol. **142**, 142 (1995).

[38] G. Iversen, Y. I. Kharkats, and J. Ulstrup, Mol. Phys. **94**, 297 (1998).

[39] Y. Lin, A. Baumketner, S. Deng, Z. Xu, D. Jacobs, and W. Cai, J. Chem. Phys. **131**, 154103 (2009).

[40] C. Neumann, in *Hydrodynamische Untersuchungen: Nebst einem Anhange uber die Probleme der Elektrostatik und der magnetischen Induktion* (Teubner, Leipzig, 1883), pp. 279–282.

[41] I. V. Lindell, *The Review of Radio Science 1990–1992* (Oxford University Press, Oxford, 1993), pp. 107–126.

[42] N. Metropolis, A. W. Rosenbluth, M. N. Rosenbluth, A. H. Teller, and E. Teller, J. Chem. Phys. **21**, 1087 (1953).

[43] D. Frenkel and B. Smit, *Understanding Molecular Simulation: From Algorithms to Applications* (Academic Press, New York, 2002).

[44] P. Linse, Adv. Polym. Sci. **185**, 111 (2005).

[45] K. Besteman, M. A. G. Zevenbergen, H. A. Heering, and S. G. Lemay, Phys. Rev. Lett. **93**, 170802 (2004).

[46] J. Pittler, W. Bu, D. Vaknin, A. Travesset, D. J. McGillivray, and M. Lösche, Phys. Rev. Lett. **97**, 046102 (2006).

[47] R. Messina, C. Holm, and K. Kremer, Comput. Phys. Commun. **147**, 282 (2002).

[48] M. Tanaka, Phys. Rev. E **68**, 061501 (2003).

[49] A. Diehl and Y. Levin, J. Chem. Phys. **125**, 054902 (2006).

[50] O. Lenz and C. Holm, Eur. Phys. J. E **26**, 191 (2008).

[51] C. Calero and J. Faraudo, Phys. Rev. E **80**, 042601 (2009).

[52] R. Messina, C. Holm, and K. Kremer, Eur. Phys. J. E **4**, 363 (2001).

[53] R. Messina, Physica A **308**, 59 (2002).

[54] K. Qamhieh and P. Linse, J. Chem. Phys. **123**, 104901 (2005).